John O. Windsor
19.5.123

OAK RIDGE NATIONAL LABORATORY

operated by

UNION CARBIDE CORPORATION

for the

U.S. ATOMIC ENERGY COMMISSION

UNION CARBIDE

ORNL - TM - 1266

COPY NO. - 11

DATE - September 7, 1965

EXPERIMENTAL SIMULATION OF LARGE, HIGH FIELD, SUPERCONDUCTING MAGNET OPERATION

W. F. Gauster, D. L. Coffey, K. R. Efferson,
J. N. Luton, H. A. Ullmaier

ABSTRACT

Diversified work has been directed toward a more thorough understanding of the complex performance of superconducting coils. Tests with sample coils wound of 0.005 in. copper clad Nb-25% Zr wire showed very different results from those made previously with 0.010 in. wire coils. The 0.005 in. Nb-25% Zr wire was used for short sample stabilization experiments which will be continued in order to clarify several newly observed phenomena. A comparison calculation between stabilized coils and conventional superconducting coils has been made. Micro Hall Probe measurements have been performed on Nb-Zr cylinders and sample coils. Calculations concerning flux distribution in hard superconductors under adiabatic field change were made.

ORNL-TM-1266

Experimental Simulation of Large, High Field, Superconducting Magnet Operation

Second Quarterly Report Covering the Period from June 1 to August 31, 1965

Prepared for

George C. Marshall Space Flight Center

National Aeronautics and Space Administration

(Government Order No. H-76798)

By

Thermonuclear Division

Oak Ridge National Laboratory

Oak Ridge, Tennessee

(Operated by Union Carbide Corporation, Nuclear Division)

W. F. Gauster, Project Supervisor,

D. L. Coffey, K. R. Efferson, and H. A. Ullmaier, Project Engineers

CONTENTS

LIST OF FIGURES

(Pages 13-24)

EXPERIMENTAL SIMULATION OF LARGE, HIGH FIELD, SUPERCONDUCTING MAGNET OPERATION

I. ABSTRACT

Diversified work has been directed toward a more thorough understanding of the complex performance of superconducting coils. Tests with sample coils wound of 0.005-in. copper clad Nb-25% Zr wire showed very different results from those made previously with 0.010-in. wire coils. The 0.005-in. Nb-25% Zr wire was used for short sample stabilization experiments which will be continued in order to clarify several newly observed phenomena. A comparison calculation between stabilized coils and conventional superconducting coils has been made. Micro Hall Probe measurements have been performed on Nb-Zr cylinders and sample coils. Calculations concerning flux distribution in hard superconductors under adiabatic field change were made.

II. 0.005-in. Nb-25% Zr SAMPLE COIL TESTS

K. R. Efferson

Quenching characteristics have been checked for coils 7.3A and 7.3B (Linde). Both coils are wound with 0.005-in.-dia Nb-25% Zr wire, with copper cladding of 0.0005 in. radial thickness, formvar insulated. Each has an ID of 4.125 in., an OD of 5 in., and a length of 0.375 in. Coil 7.3A has 2549 turns while 7.3B has 2551 turns.

Critical current data obtained with these two coils show relatively high scattering. The quenching characteristics of these coils deviates appreciably from those previously obtained with a coil having 2250 turns wound with 10 mil Nb-25% Zr wire.[1] In the latter case, at zero field only, large training and scattering was observed. Furthermore, the quenching current characteristics showed minima and maxima, both for

[1] ORNL-TM 1083, March 23, 1965, p. 30.

aiding and opposing fields. With the coils 7.3A and 7.3B, the scattering and training zone was not restricted to zero field and the quenching characteristic decreased monotonically with increasing field. These tests will be continued and attempts will be made to reduce the scattering by improving the mechanical design.

III. STABILIZED 0.005-in. WIRE SHORT SAMPLE TESTS

K. R. Efferson

The sample is a 0.005-in.-dia copper clad Nb-25% Zr wire, 10 in. long, indium soldered to a copper strip 0.003 in. thick, 3/16 in. wide, and 14 in. long. Voltage contacts have been made to the indium solder adjacent to the superconducting wire. The sample has been mounted on a hold in form of a hairpin which is 1 in. wide and 4.7 in. long. The potential across the sample was plotted on the X axis and the current on the Y axis of an X-Y recorder. Measurements were made by raising the current at a constant rate in a fixed magnetic field until the sample went normal. Thereafter the current was lowered at the same rate.

Figure 1 shows typical experimental results. At zero field (Fig. 1a) with increasing current a small potential appeared across the sample until the potential changed suddenly to a higher value. With a further increase of the current the potential rose at a higher rate. When the current was lowered the voltage decreased approximately uniformly until at a lower state a jump to the initial voltage characteristic occurred. When repeating this experiment the upper critical current showed an appreciable training effect, while the lower critical current remained nearly constant. The extent of the training is shown by comparing Fig. 1a and 1b, which represent the first and 15th of the zero field tests. The first part of the I-V characteristics corresponds to a resistance of 8 $\mu\Omega$, and the second to approximately 32 $\mu\Omega$.

These results are tentatively interpreted as follows: Initially the Nb-Zr wire is in superconducting state and approximately at the bath temperatures of 4.2°K. The measured potential is a voltage drop due to a current component flowing through indium solder and copper.

When reaching the quenching current of 55 amps (Fig. 1a) the wire becomes normal and the current flows through the copper strip. This transition is very sharp. Further increase of the current raises the temperature of the copper ribbon and of the Nb-Zr wire. When the current is decreased to 55 amps the ohmic heating of the copper strip maintains the temperature at too high a value to allow the Nb-Zr wire to return to the superconducting state. At 43 amps a sudden potential reduction occurs which indicates that the wire again became superconducting.

A different performance has been observed at fields of around 5 kilogauss (Fig. 1c). The I-V diagram does not show any irreversible behavior. A characteristic trace is exactly repeated when the current is increased and decreased. At intermediate fields ($6\ kG < H < 20\ kG$) the loop characteristic (similar to Fig. 1a) occurs again. At higher fields the I-V curve is reversible and the shape resembles Fig. 1c; however, without pronounced spikes.

These preliminary tests will be continued with refined experimental arrangements.

IV. COMPARISON CALCULATION BETWEEN STABILIZED AND CONVENTIONAL SUPERCONDUCTING COILS

W. F. Gauster

Soon after the phenomenon of degradation was observed, systematic efforts were made to overcome this difficulty. For example, R. W. Boom[2] investigated superconducting coils with copper secondary windings;

---

[2] R. W. Boom, L. D. Roberts, and R. S. Livingston, "Developments in Superconductive Solenoids," High-Energy Instrumentation Conference, Geneva, July 16-18, 1962.

Betterton and Kneip[3] reported that a solenoid wound with 0.006-in. Nb-25% Zr wire which was covered with an inconel mantle of 1 mil radial thickness displayed short sample performance. Later, copper clad Nb-Zr and Nb-Ti wire which show reduced degradation effect became commercially available. In all these cases the use of non-superconducting metals in close connection with the superconducting winding material reduces flux jumps and improves appreciably the quenching characteristic of the superconducting coil.

Another observation was made by several researchers: Metallurgical treatment which improved the short sample characteristic of the superconductor shows sometimes definitely derogative effects on the coil performance ("overbred" superconductors). This kind of material displays disastrous flux jumps and the need for a stabilization of the wire performance becomes obvious.

Recently decisive steps in the art of building stabilized superconducting coils were described by T. H. Field and Charles Laverick,[4] and Z. J. J. Stekly and J. L. Zar.[5] In both cases the essential point was to choose intentionally very low packing factors. For superconducting coils with small α-values (ratio of outside to inside diameter; not to be confused with Stekly and Zar's[5] stability parameter α) a decrease of the packing factor λ corresponds to only a small increase of the length of the superconducting winding material. In other cases, however, it is necessary to consider the inter-relation between coil geometry, the short sample characteristic, and the degradation in order to decide whether or not a stabilized coil might be superior to a conventional superconducting coil with a relatively high packing factor. Of course, an important

---

[3] J. O. Betterton, Jr., G. D. Kneip, D. S. Eason, and J. O. Scarbrough, "Size Effect and Interstitial Impurities in Nb_3Zr Superconductors. Superconducting Solenoids with Metal Insulation." Superconductors, Editors, M. Tanenbaum and W. Wright, Proc. AIME, Feb. 1962, Interscience Publ., 1962.

[4] T. H. Fields and Charles Laverick, "Some Supermagnet Design Considerations," IEEE Transactions on Nuclear Science, NS-12, June 1965 pp. 362-366.

[5] Z. J. J. Stekly and J. L. Zar, "Stable Superconducting Coils," IEEE Transactions on Nuclear Science, NS-12, June 1965, pp. 362-366.

advantage of stabilized coils is the avoidance of an uncontrolled transition to the normal state with the resultant loss of magnetic field and liquid helium. On the other hand, the increased coil volume calls for a large Dewar volume and larger liquid helium losses during the initial cooling of the superconducting coil.

In the following, one special case shall be discussed which illustrates well the above mentioned points of view. Stekly and Zar[6] tested a stabilized coil consisting of 14 "pancakes" with ID = 5 in., OD = 17 in., each pancake 0.5 in. wide. Due to 13 interspaces between the pancakes, the total coil length, 2b, was 13 in. The conductor was a copper strip 0.040 in. by 0.5 in. cross section with nine longitudinal grooves into which nine strands of 0.010 in. Nb-25% Zr wire were inserted. This superconducting wire was metallurgically "overbred" with a short sample quenching current of 85 to 110 amps at 40 kilogauss.

A comparison of such a stabilized coil with a conventional superconducting coil can be made easier if we assume that the 14 pancakes are arranged without interspaces, i.e., length 2b = 7 in. and $\beta = 2b/ID = 0.75$ (β should not be confused with the parameter β as introduced by Stekly and Zar[5] Eq. 14). In this way a coil with uniform current density is obtained.

Stekly's conductor arrangement with insulation between turns has a packing factor λ of about 0.03. Let us first assume that a Nb-25% Zr wire with the following short sample quenching data was used*:

Table 1

H (kilogauss)	10	15	20	25	30	35	40	45	50	55	60	65	70
I (amps)	90	70	60	56.3	54	52	50	46.5	40	32	22	13	3.5

A simple calculation procedure yields for this coil (without consideration of the degradation effect) a quenching current of around 52 amps (or 468 amps in the 9-wire conductor) producing at the inside coil surface $H_M = 35.2$ kG, at the coil center $H_o = 32.6$ kG.

---

[6] See reference (5) and Dr. Z. J. J. Stekly's oral communication.

*Copper clad Supercon wire.

As has been mentioned previously, Stekly and Zar employed Nb-25% Zr wire with very high short sample quenching currents. For our calculation we will use twice the quenching currents of Table I. Thus the following values are obtained:

H_M = 51.2 kG; H_o = 47.5 kG; I = 75.5 amps (9 I = 680 amps).

This coil has a volume factor $v = 2\pi(\alpha^2 - 1)\beta = 93$. With a packing factor $\lambda = 0.5$ the same quantity of superconducting material corresponds to a volume factor

$$v^* = \frac{0.03 \times 93}{0.5} = 5.58$$

A volume optimized coil with this volume factor has $\alpha = 1.48$ and $\beta = 0.75$; i.e., with ID = 5 in., OD = 7.4 in. and length 2b = 3.75 in. Without degradation the wire characterized by Table 1 yields

$$H_M = 59.3 \text{ kG}; \quad H_o = 46.0 \text{ kG}; \quad I_c = 23.2 \text{ amps}.$$

Based on tests with similar superconducting coils, a critical current of 20 amps can be expected. This corresponds to H_M = 52 kG and H_o = 40.3 kG.

This volume optimized, unstabilized coil generates in its center a field which is 15% smaller than that produced by the stabilized coil with an equal quantity of superconducting material (different short sample performance assumed). Of course, the field homogeneity of the stabilized coil is much better. Furthermore, as mentioned previously, current increase beyond the critical value of the stabilized coil has no drastic consequences. However, the advantages of the small coil and Dewar volumes must also be considered. Finally, it is obviously an advantage to operate with 20 instead of 700 amps.

This calculation illustrates well the advantages of a stabilized coil design in this special case. However, more and refined investigations are necessary to draw general conclusions.

V. A. MICRO HALL PROBE MEASUREMENTS ON A CYLINDER

K. R. Efferson

Field distributions in a cold worked Nb-25% Zr rod are being investigated in longitudinal magnetic fields at 4.2°K. The sample is a 4-1/8-in. long and .26-in.-dia solid cylinder which has been split into two equal

pieces by cutting perpendicular to the longitudinal axis. The cylinder is then mounted in such a way that the gap between the two halves is 0.004 in. A mechanical system moves a Micro Hall probe (see the following section) through the gap to measure the magnetic field as a function of position. The position of the Probe is determined electrically so that field magnitude vs position can be plotted on an X-Y recorder.

The field in a cylinder without a gap is, of course, different from that measured with our arrangement. Since the ratio of gap width (0.004 in.) to rod diameter (0.26 in.) is very small, a field disturbance can be expected only near the cylinder surface. This zone is, however, of special interest, and calculations are being made to estimate the possible influence of the gap disturbance. The following measurement results have not been corrected for fringe effects.

Some characteristic field measurements are represented in Fig. 2. By means of a bifilar heater winding, the sample was driven normal in zero external field, and after cooling of the sample the external field was raised to 5 kilogauss (Fig. 2a). Keeping this external field constant the sample was again heated and cooled so that the field of 5 kilogauss penetrated the entire sample. When increasing the external field to 10 kilogauss, curve b was obtained. Finally curve c shows the flux distribution with an external field of 14 kilogauss after flux penetration at 10 kilogauss. As to be expected, from Kim's formula

$$J = \frac{\alpha}{B + B_o}$$

the local current density J decreases with increasing B. The numerical values of the current density as calculated from these measurements are in the same order of magnitude found by other authors.

This field scanning method is also convenient for studying flux jumps in hard superconducting cylinders. Figure 3 shows the following example: First, the sample was heated and cooled in an external field of -1.5 kilogauss (curve a). After raising the external field to +4 kilogauss the flux distribution b was obtained. Lowering the external field to zero yielded the distribution curve c. The distribution is

far from axisymmetric. Furthermore, when lowering the external field from +4 kilogauss to zero the field distribution up to a certain radius remained unaffected.

These flux distribution measurements will be continued.

B. MICRO HALL PROBE MEASUREMENTS ON A SAMPLE COIL

D. L. Coffey

An experimental arrangement has been constructed which permits sweeping a Micro Hall Probe through a small (0.013 in.) slit in the midplane of a superconducting coil. The slit dimension is approximately one wire diameter. The coil geometry and the probe arrangement are shown in Fig. 4. This arrangement of the probe positioning device allows a small (0.04 mm^2) Hall element to sweep through an arc passing radially through the bore of the coil (Fig. 4, curve BC), two internal sections (AB and CD) and a small part of the external field (AA' and DD'). The sweep speed is adjustable through a gear arrangement outside the Dewar (range 30 min/sweep to 1/2 min/sweep).

A new type of Micro Hall Probe has been developed.[7] The probe used here is tailored to the requirements of this experiment and has the following significant features:

Material	Indium Arsenide
Cover	Silicon Monoxide
Sensitive Area	0.04 mm^2
Total Thickness	0.03 mm
Sensitivity	5×10^{-4} volt/amp gauss
Impedance	2000 Ohm
Linearity	5% of Full Scale to 50 Kilogauss

Field measurements have been made with the Hall Probe connected either directly to an X-Y recorder or with an amplifier between the probe and the recorder.

---

[7] J. E. Simpkins, "Investigations on the Possibility of Using Indium Arsenide Films for Cryogenic Hall Probes," ORNL Thermonuclear Division Semiann. Prog. Rept. for Period Ending April 30, 1965 (ORNL-3836).

Examinations to date have included only the self fields generated by the superconducting coil. Later experiments will be made with superimposed external fields.

The midplane field of a non-superconducting (e.g. copper) coil with dimensions and turns equal to that of the superconducting coil is shown in Fig. 5 (curve a). The effect of a 0.013-in. gap between sections is shown (curve b). This curve is the starting point for the analysis of the effects of the diamagnetic currents in the superconducting coil.

In a superconducting coil it can be expected that the diamagnetic behavior of the wire will distort the field. As the current is increased, flux penetration of the wire results, and the field distributions approach more closely that of a non-superconducting coil. This effect is apparent in Fig. 6. The influence of the diamagnetic currents is seen in the shape of the field within the bore of the coil. At low currents where the diamagnetic fields are important, a convex shape is observed. At higher currents the field shape becomes concave as in a non-superconducting coil. In order to study field shape at low currents in more detail an additional amplifier between the Micro Hall Probe and the recorder has been used. The field shape recorded is shown in Fig. 7. The coil current is 2 amperes and the calculated maximum self field in a corresponding non-superconducting coil is 2084 gauss. An appreciable deviation from the field shape of the superconducting coil from that of the corresponding non-superconducting coil can be seen. In a (infinitely) long superconducting coil, the coarse-grained average midplane field is identical with that of a non-superconducting coil.[8] For a short superconducting coil, however, the diamagnetic currents cause first a rapid drop in field intensity as one proceeds from the inside toward the outside surface. Thereafter the field gradient is smaller than that in the non-superconducting coil (Fig. 7). This observation can be understood qualitatively if one considers that the

---

[8] B. S. Chandrasekhar, W. F. Gauster, J. K. Hulm, "Degradation Factor and Diamagnetic Currents in Supermagnets, APL, Vol. 2, No. 11, pp. 228-9, June 1, 1963.

diamagnetic currents are more intense in the inside than in the outside layers.[8] Therefore the return path of the diamagnetic field superimposed on the transport current field produces a negative field component decreasing from the inside to the outside layers.

In Figs. 6 and 7, field ripples are clearly evident. Their number is approximately one-half of the number of layers. Visual examination of the winding end planes of a similarly wound coil shows that alternate layers are generally displaced one-half of one wire diameter. A more thorough investigation of these ripple fields is planned.

Figure 8 shows the remanent fields with zero applied current after successively energizing the coil to 2, 4, 6, 10, 20, and 30 amps. Magnetic moment measurements on bundles of 0.010 in. Nb-25% Zr wires[9] showed that a field of about 5 kilogauss is necessary to reach maximum magnetization. This corresponds to the observation on the superconducting coil that for fields of 5 kilogauss or more, the remanent magnetization (i.e., the field after raising and lowering the transport current) remains constant. In accordance with this result, Fig. 8 shows that maximum remanent fields are trapped over a radial distance where the maximum transport current field has reached or exceeded about 5 kilogauss. This seems to explain the change of the shape of the remanent field from a nearly triangular form to almost rectangular shape.

The remanent fields shown in Fig. 8 were obtained after reaching a maximum transport current field without occurrence of a normal transition (quenching). Other measurements were made to investigate the remanent fields after quenching. The quenching currents were between 30 and 44 amps; irregular training effects have been observed. Several of these remanent fields are shown in Fig. 9. They partly resemble remanent fields obtained without quenching but with much smaller maximum currents. For instance, curve a was obtained after quenching with 44.1 amps and is similar to a non-quenching distribution with approximately 3 amps maximum current. Figure 9b represents a remanent field after quenching with 33.7 amps. Only the outside regions have trapped

---

[9] D. C. Hopkins and W. F. Gauster, "Magnetic Moment Measurements on Nb-Zr Wires," ORNL Thermonuclear Division Semiann. Prog. Rept. for Period Ending Oct. 31, 1963 (ORNL-3564).

a remanent field. Finally in Fig. 9c, almost no remanent field can be seen. Remanent fields in the mid-plane of a superconducting coil are, of course, not indicative of the total state of the coil.

The physical processes which lead to the different remanent fields after successive quenchings are rather complicated. It is intended to combine oscigraphic measurements with these field scannings.

The Micro Hall Probe in the coil mid-plane complement the investigations of Aron,[10] who studied the axial fields of superconducting coils. He discussed in detail the close correlation to the volume magnetization of the superconducting windings. The Micro Hall Probes are a very effective tool for the measurement of the fine structure of the fields produced by superconducting coils. Similar attempts have been made with ballistic methods.[11]

VI. LARGE VOLUME COILS OF THE ORNL MAGNET LABORATORY

J. N. Luton, Jr.

A previous report[12] described magnet coils in use in the laboratory, and also a large bore coil (C_1) now under construction. The C_1 coil is to be a power-optimized coil of 8th order, producing a homogeneous field of about 60 kG over a volume of nearly one cubic foot. The coil is to be essentially as previously planned, except for the addition of low current shunts around some pancakes to tailor the current density distribution more exactly. This greatly improves the calculated field homogeneity, as can be seen by comparing Fig. 10 of this report with Fig. 18 of the previously cited report.

Construction has recently begun on another coil set also designed to produce a homogeneous field over a large volume. This set will consist of two identical coils, D_1 and D_2, each with a bore of 13 in., an outer diameter of 36 in., and a length of 13 in. At a power level of 6-1/2 megawatts and a coil spacing of 1-1/2 in., the assembly will produce a

[10] Paul R. Aron, "Magnetization and a Superconducting Solenoid," UCRL-10854 (June 5, 1963).

[11] B. Taquet, personal communication.

[12] Appendix I of ORNL-TM-1083.

field strength of 63 kG. This distance was intentionally chosen slightly smaller than the gap width which corresponds to the "Helmholtz Condition" (zero condition for the second term in a Legendre polynomial development). This arrangement provides somewhat better field homogeneity in the mid-plane by sacrificing some field quality along the axis. As can be seen in Fig. 11, the field strength contours of the D coils are not quite as impressive as those of Fig. 10; but the field is homogeneous enough for most of the intended experiments.

Since the current density in the coil windings is everywhere constant, the winding design is simple and economical. Furthermore, the assembly, consisting of a pair of coils separated by an axial gap of variable length, provides mid-plane access to the experimental volume and flexibility of field arrangement. Finally, the mechanical structure will be able to withstand operation with the coil currents opposing. The resulting cusp configuration will provide high field gradients, large radial fields, and, with proper coil spacing, a large region of uniform field gradient, all of which are expected to prove valuable in future experiments.

If one is concerned only with the magnitude of the flux density $\overline{B}$ at any point, then Fig. 11 describes the field of the D coils adequately. However, for some purposes the relevant parameter is the magnitude of the vector difference between $\overline{B}$ and the field $\overline{B}_o$ (the field at the coil center) in which case the $\left|\Delta\overline{B}\right|$ contours of Fig. 12 describe the field in a more useful way.

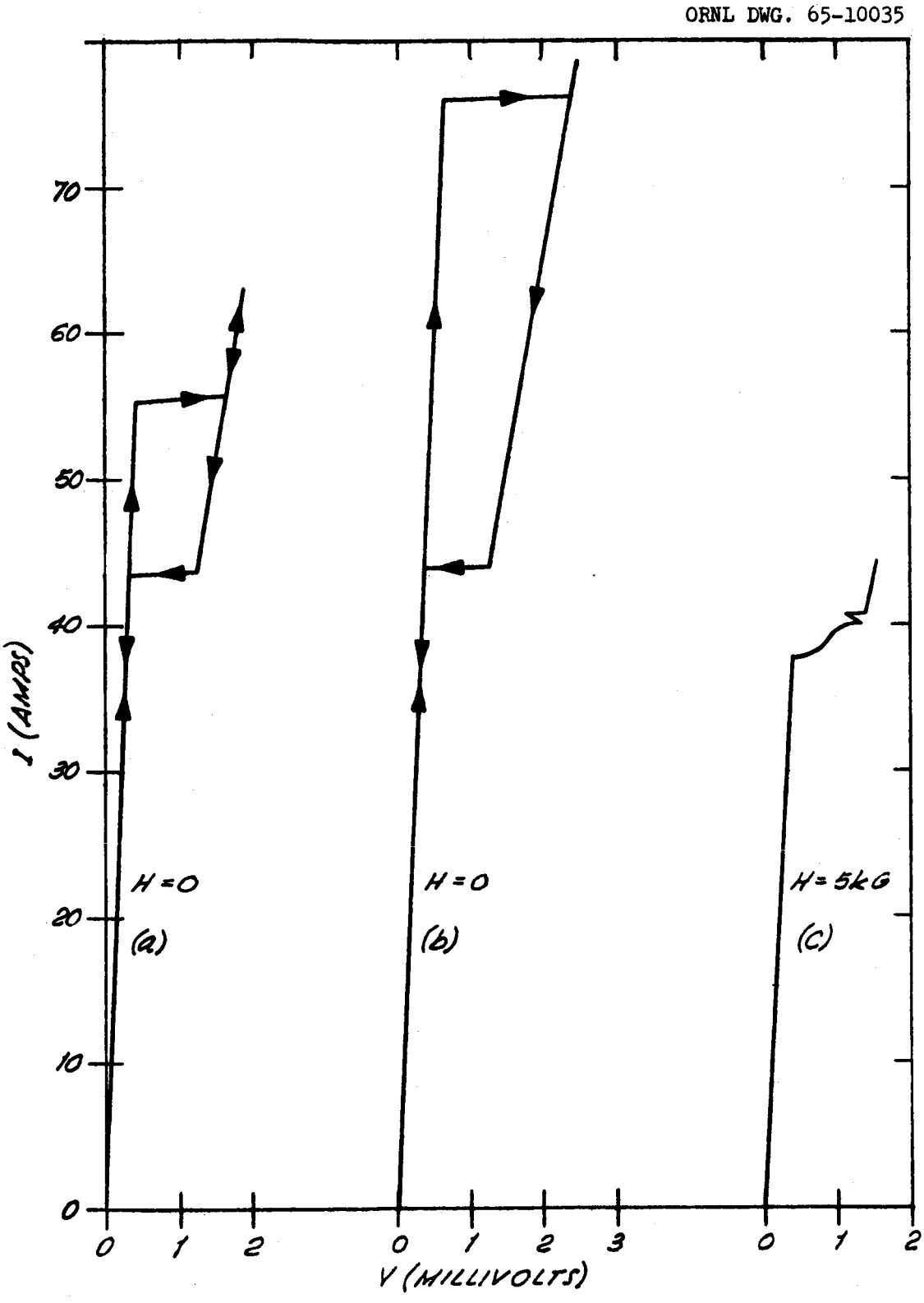

Fig. 1. Current vs Potential for Stabilized Short Sample.

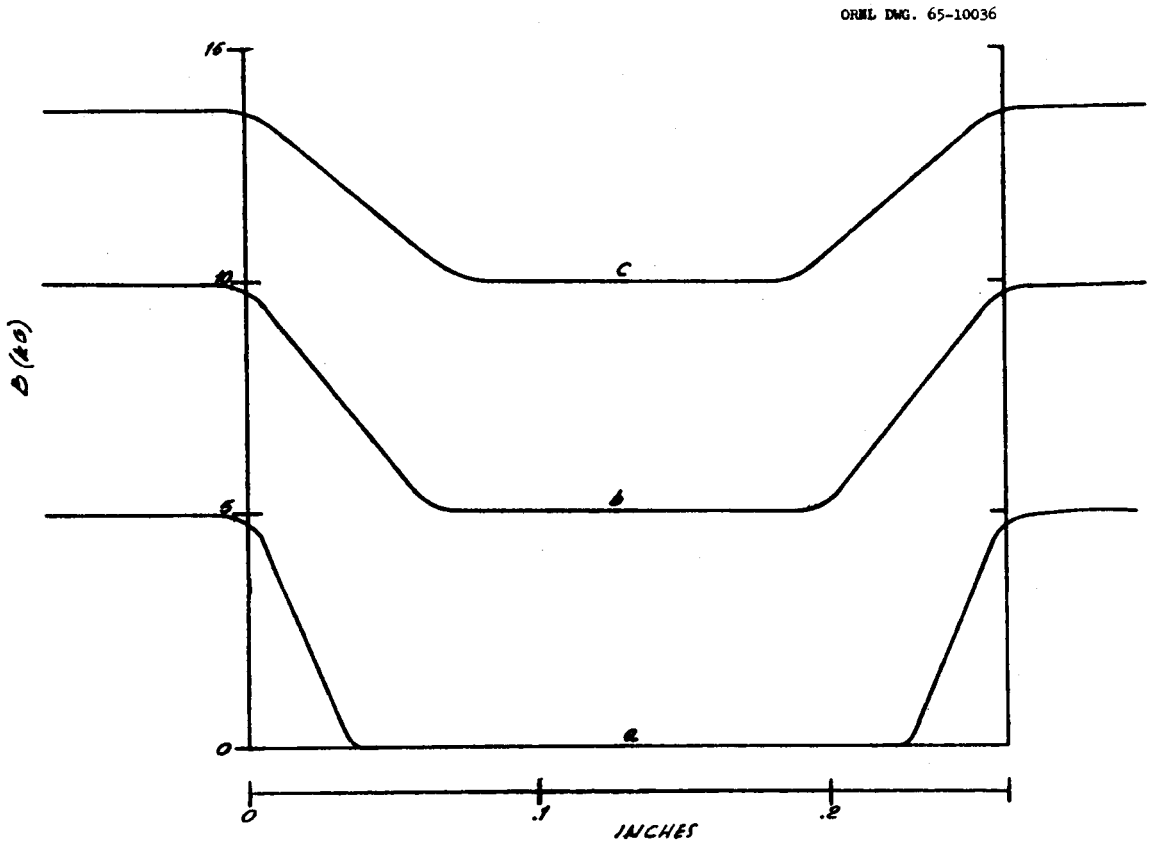

Fig. 2. Change in Flux Distribution with External Field.

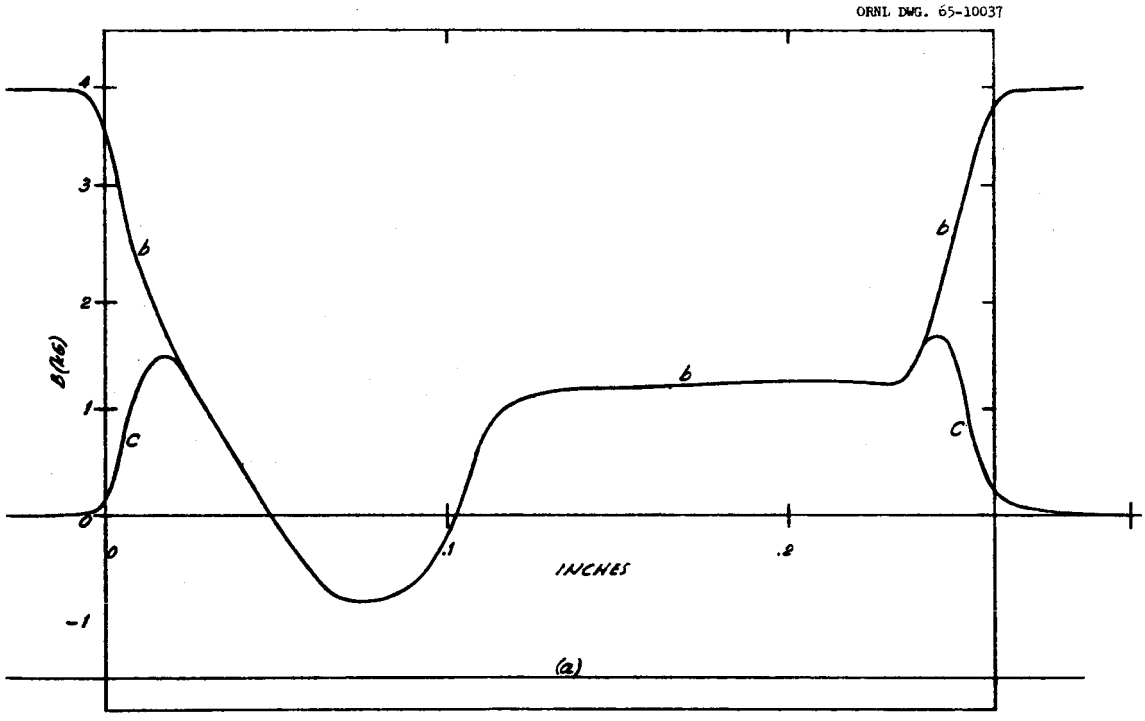

Fig. 3. Flux Jumps Obtained with Low Internal Fields.

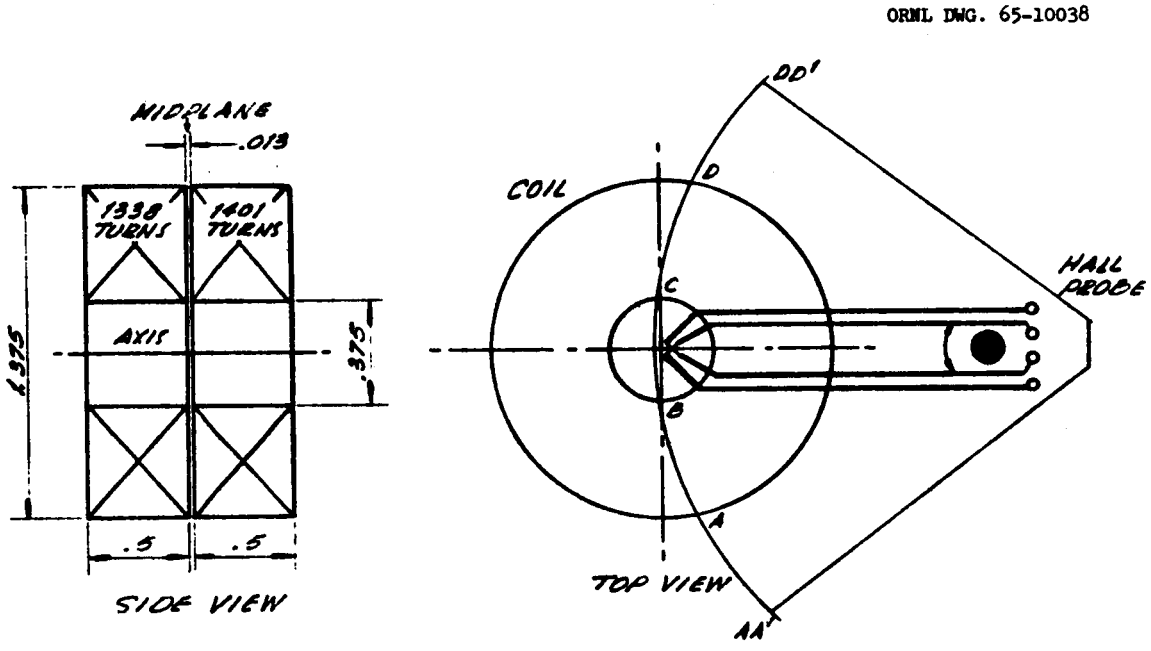

Fig. 4. Probe Arrangement for Field Measurement in Midplane of a Superconducting Coil.

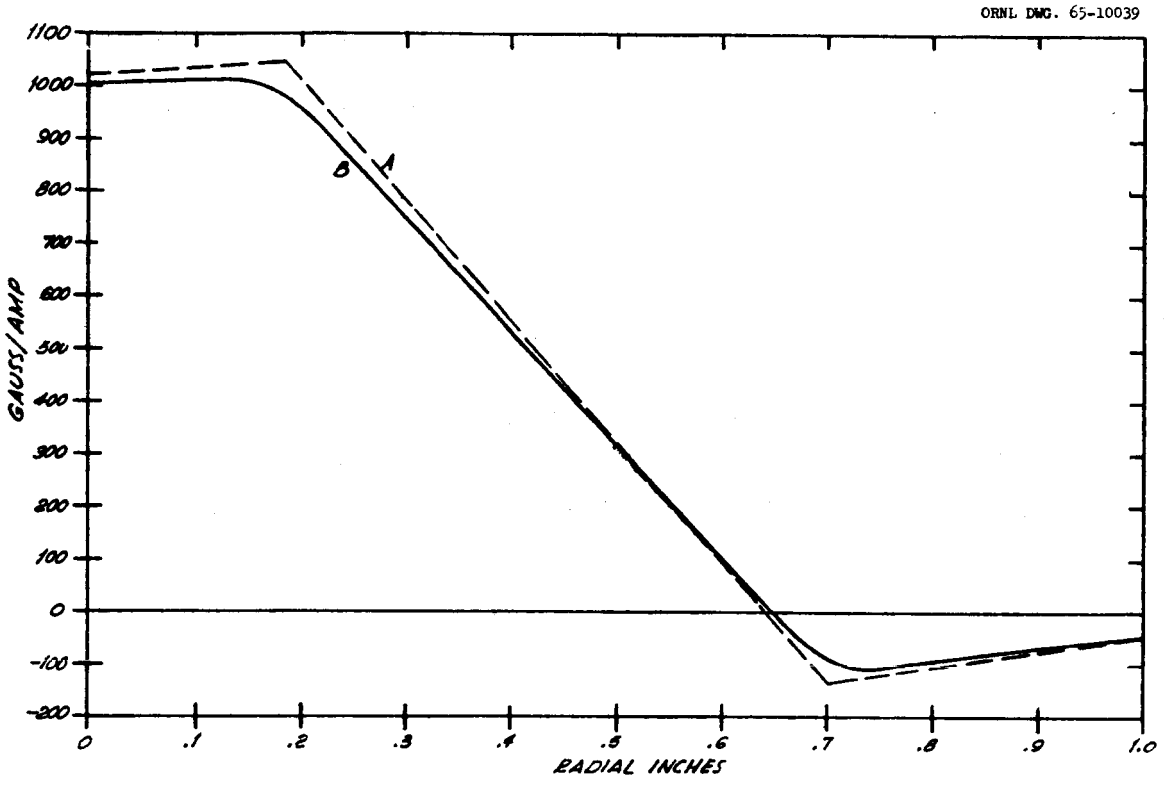

Fig. 5. Calculated Midplane Field of a Non-Superconducting Coil with the Dimensions of Fig. 4.

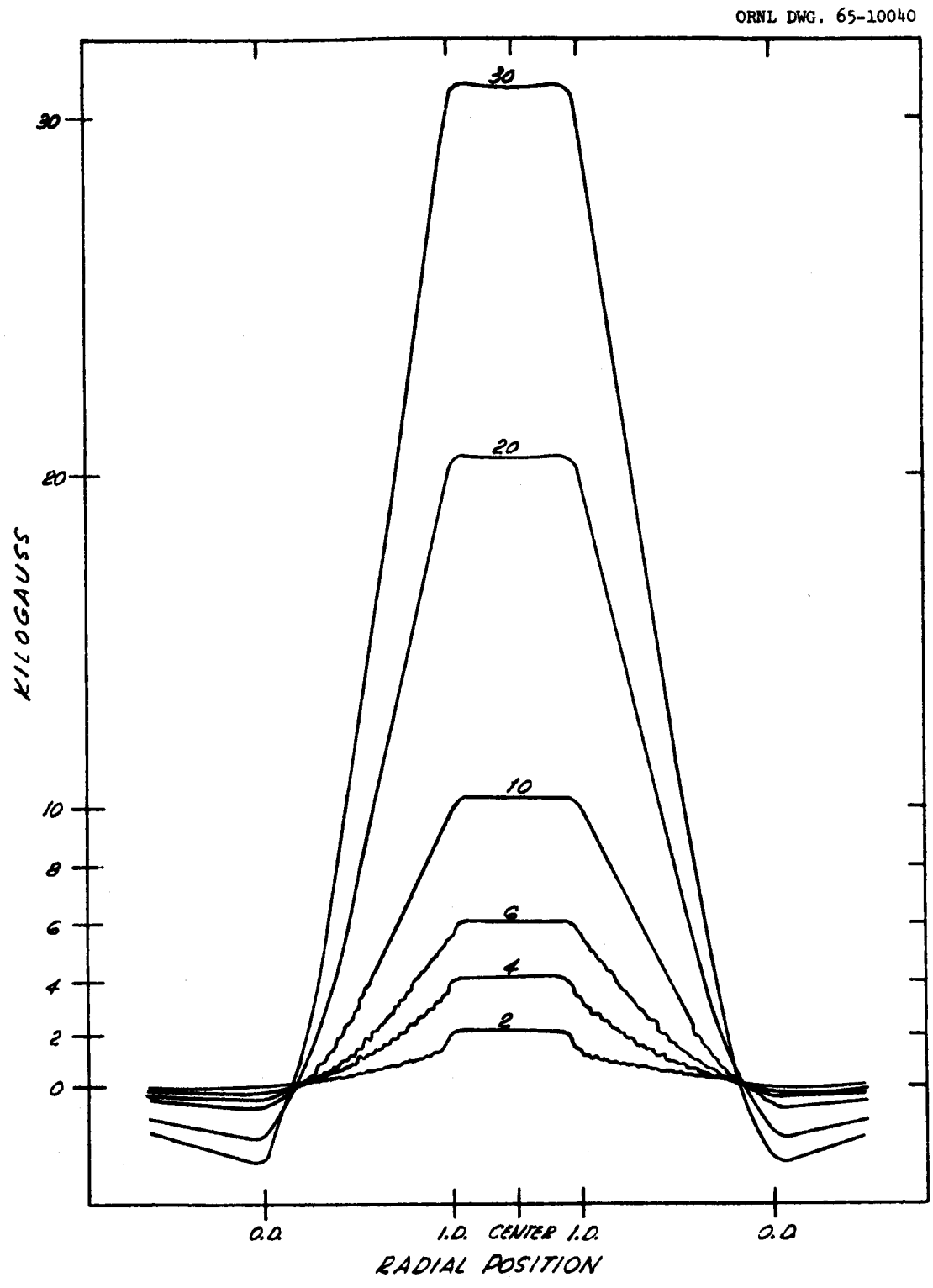

Fig. 6. Virgin Coil. Midplane Field Scan with Transport Currents from 2 to 30 Amps.

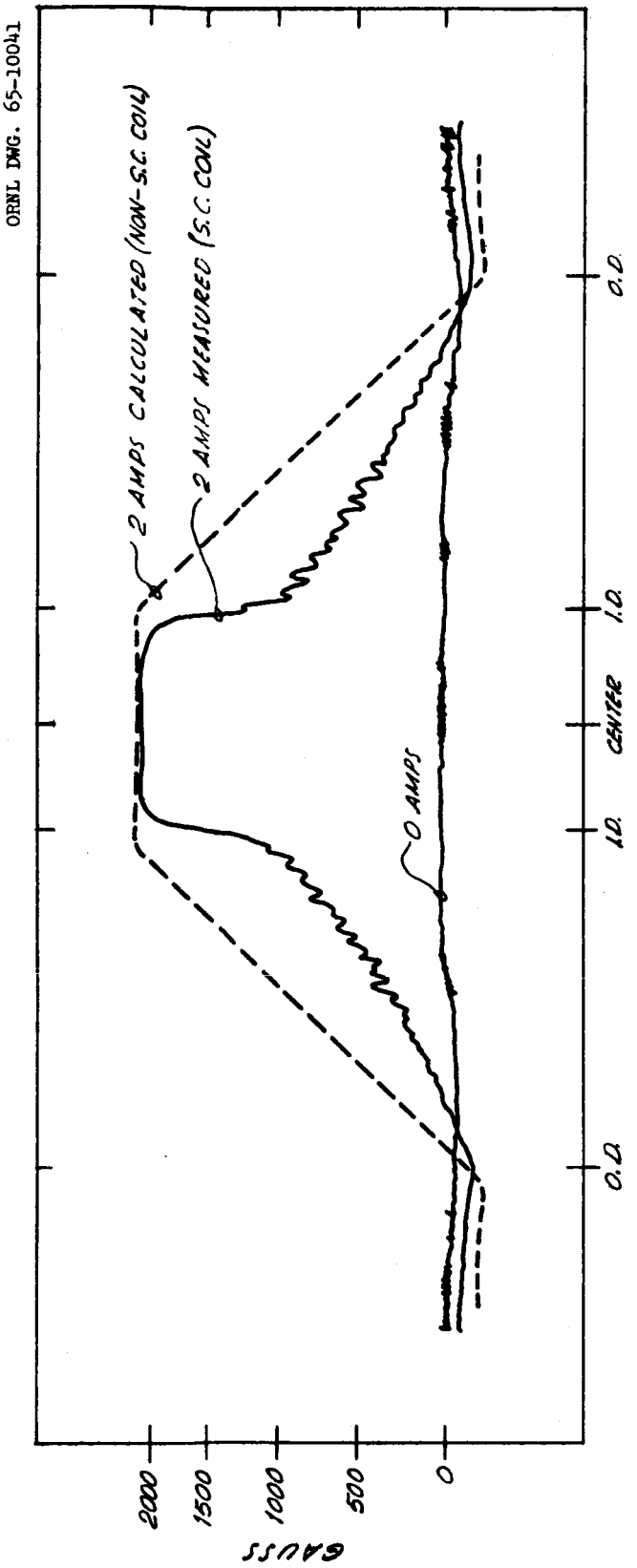

Fig. 7. Coil Midplane Self-Field with 2 Amp Transport Current.

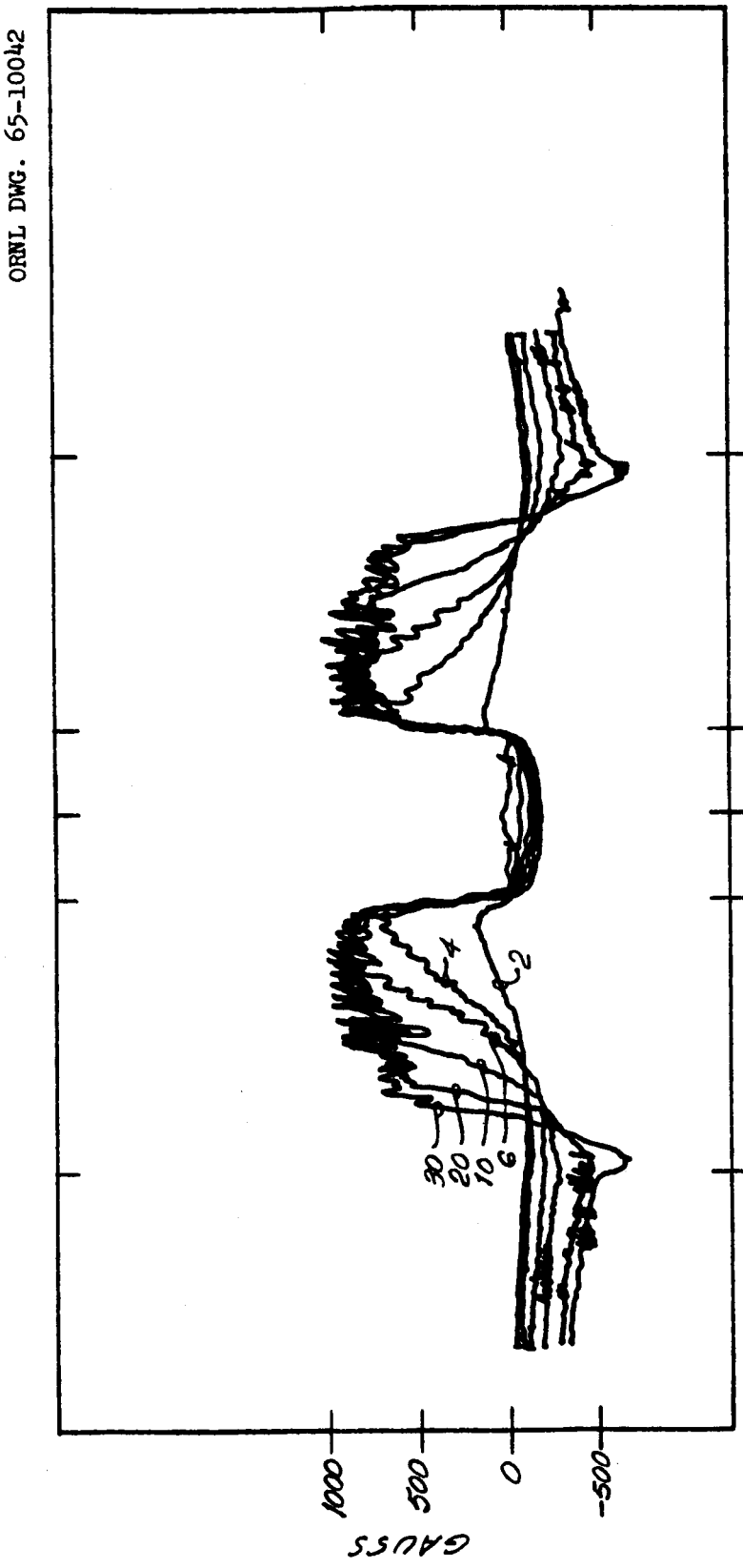

Fig. 8. Remanent Fields after Peak Transport Currents of Fig. 6 without Quenching Transitions.

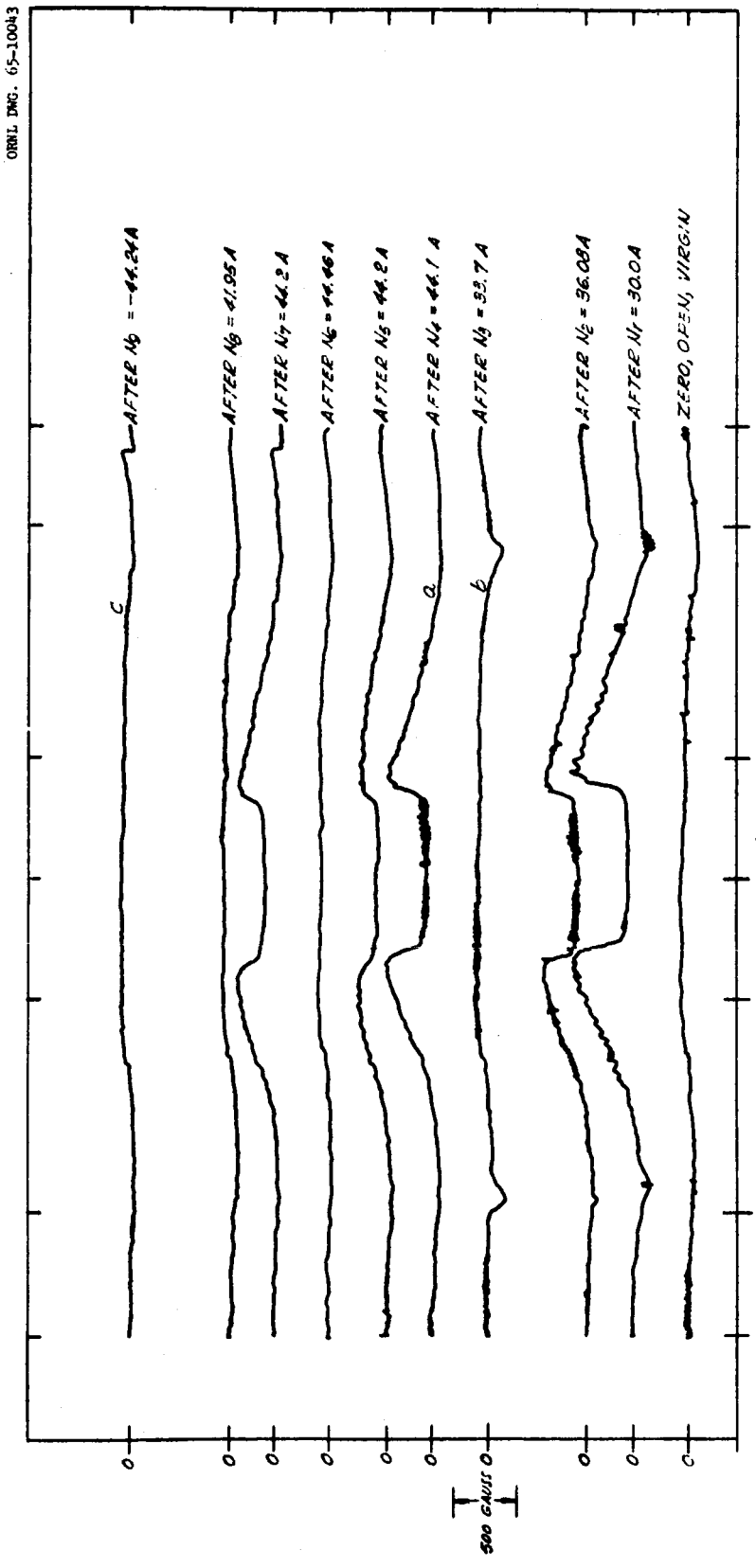

Fig. 9. Remanent Fields after Successive Normal Transitions.

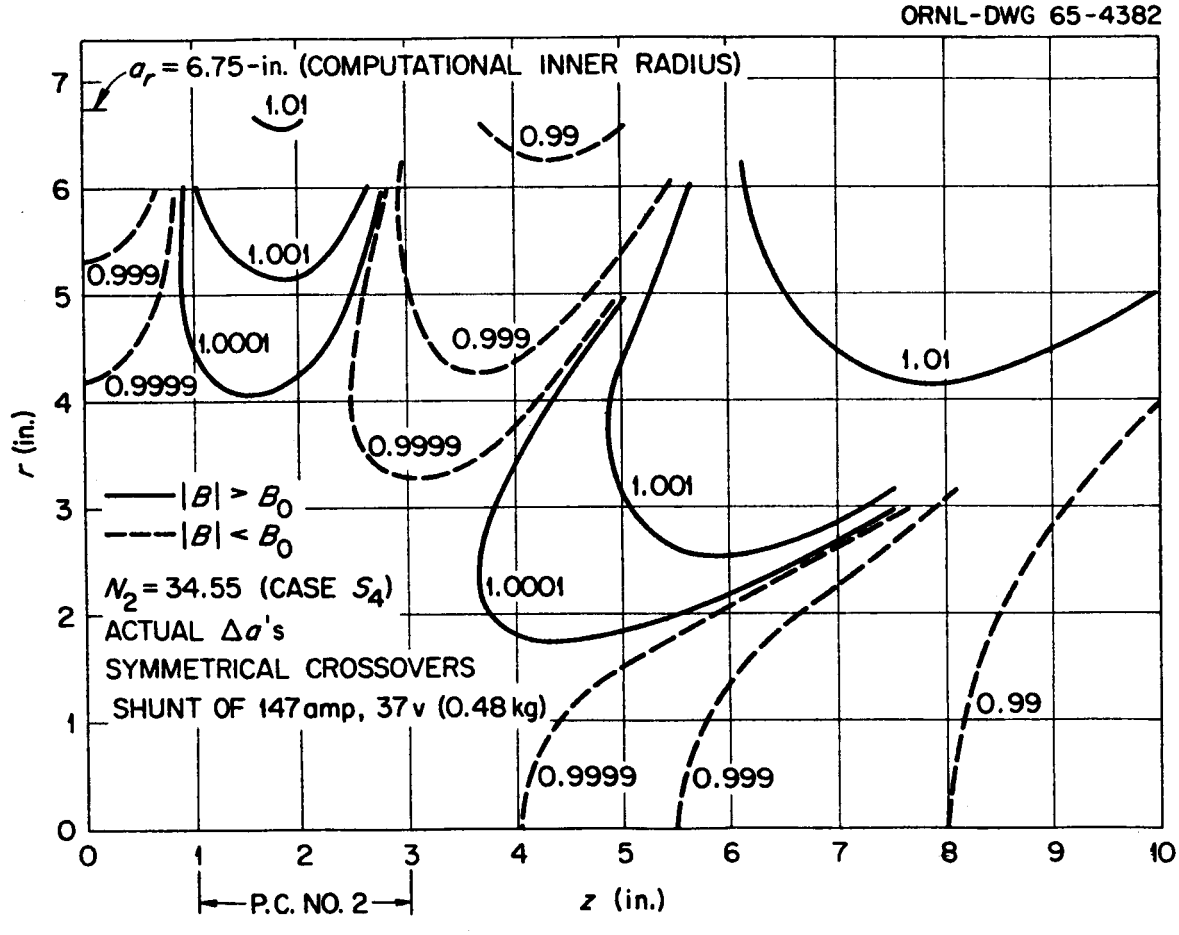

Fig. 10. Constant |B| Contours for C-1 Coil with Shunt.

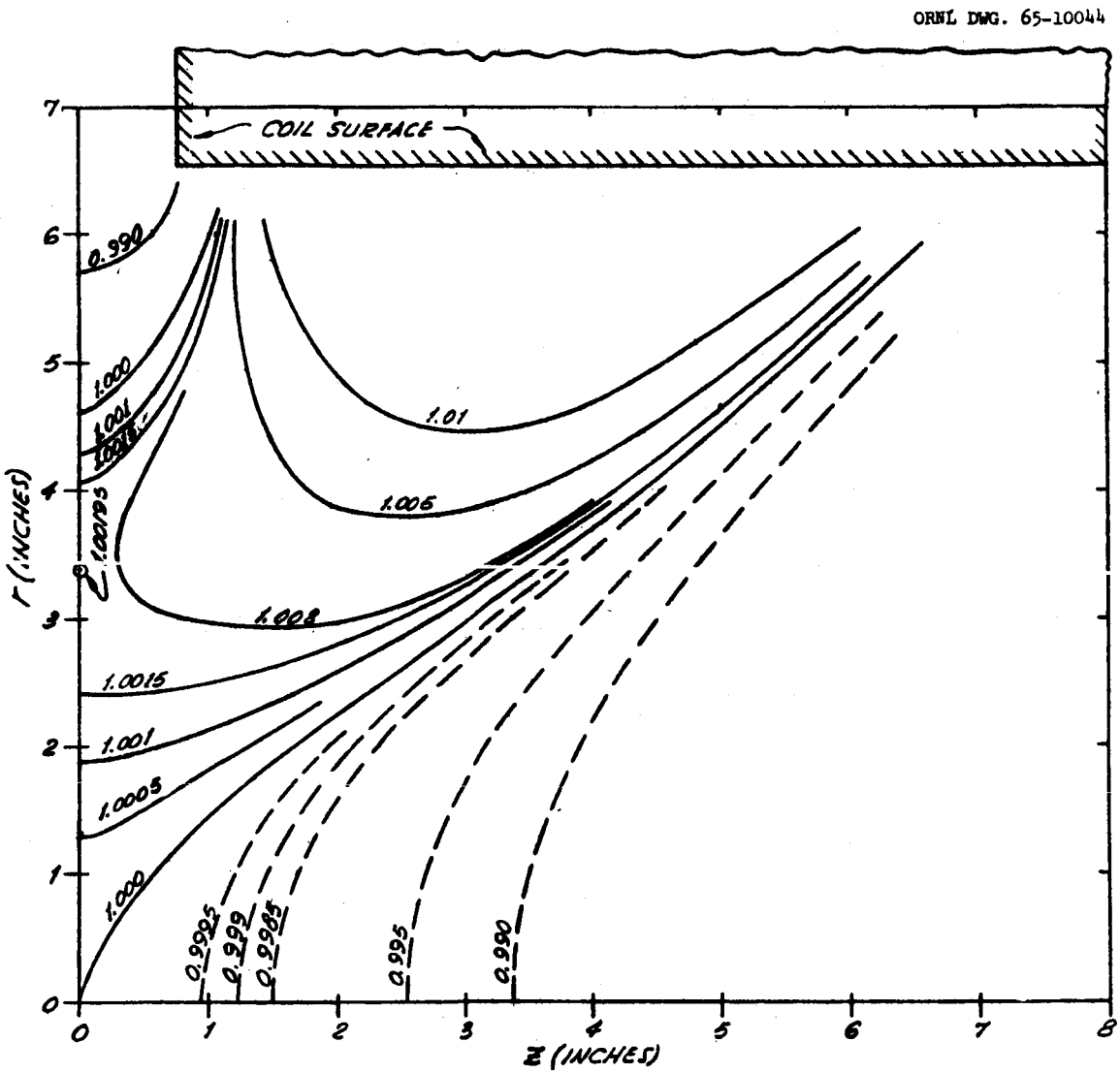

Fig. 11. |B| Contours for D Coils with 1-1/2-in. Gap.

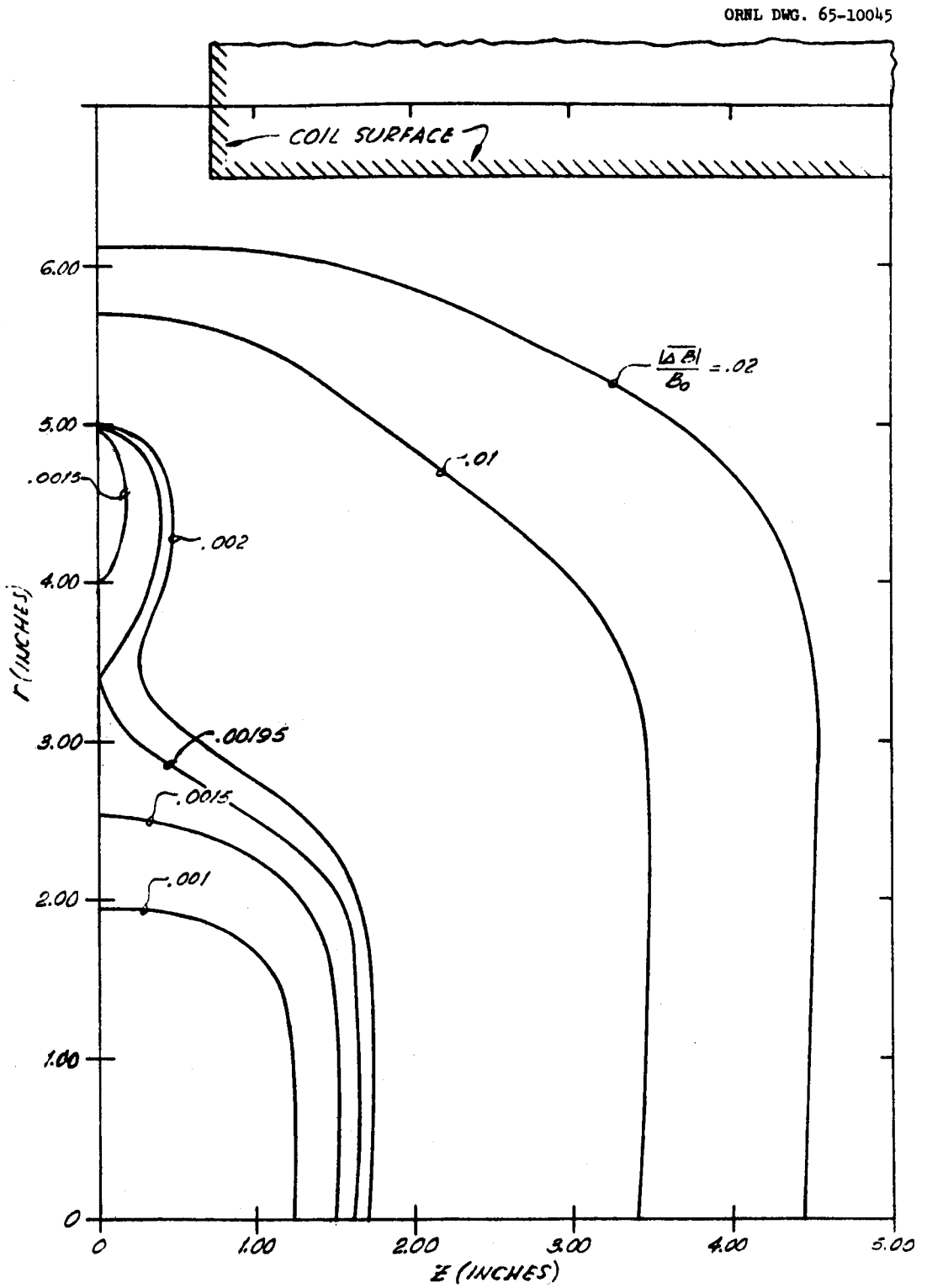

Fig. 12. $\left|\overline{\Delta B}\right|$ Contours for the D Coils with 1-1/2-in. Gap.

APPENDIX A

FIELD DISTRIBUTION IN A HARD SUPERCONDUCTOR WITH ADIABATIC FIELD CHANGE*

W. F. Gauster and H. A. Ullmaier

I. INTRODUCTION

If a longitudinal field around a hard superconducting cylinder is adiabatically raised, flux penetrates. The distance ξ of the flux front from the surface is a time dependent function $\xi(t)$. As Wipf and Lubell[1] mention, the speed of the flux front is

$$v_{ff} = \frac{d\xi}{dt} = \frac{\frac{\partial B}{\partial t}}{\frac{\partial B}{\partial \xi}}$$

B stands for the flux density.

The distance of a point inside the wave from the wave front is x. Of course, $x \leq \xi$. The distribution of any quantity, say B, inside the wave is in general a function of x and of the time t

$$B = B(x,t).$$

The change of flux will induce an EMF. The maximum value of the electric field strength E occurs on the surface of the cylinder:

$$2 \pi R E = - \frac{d\phi}{dt} \qquad (1)$$

Since E has the same direction as the shielding current density J, an energy per unit volume of

$$dW = - E J \, dt = \frac{J}{2 \pi r} \, d\phi \qquad (2)$$

---

[1] S. L. Wipf and M. S. Lubell, Phys. Letters, 16, 103 (May 15, 1965).

*Research sponsored by the U. S. Atomic Energy Commission under contract with the Union Carbide Corporation.

is dissipated. The energy necessary to accelerate the electrons is neglected. This leads to a temperature rise dT. Under adiabatic conditions

$$\frac{J}{2\pi r} \, d\phi = c(T, B) \, dT \tag{3}$$

c(T, B) is the specific heat in the superconducting state at the temperature T and the field B.

II. FIELD DISTRIBUTION IN A SEMI-INFINITE SLAB

First we consider a hard superconducting semi-infinite slab ($r \to \infty$) with zero initial conditions (the whole material in "virgin state," i.e., B = 0 and T = T_o). The following step by step method could be used for determining the distributions of B, T and J. The designations in Fig. 1 are self-explanatory. For the wave front

$$\frac{\partial B}{\partial x} = \mu_o \, J(T, B) = \mu_o \, J \, (T_o, 0) = \mu_o \, J_{bo} \tag{4}$$

is constant. Therefore (for sufficiently small s)

$$B_{10} = B_{21} = B_{32} = \text{---} = \mu_o s \, J_{bo} \tag{5}$$

The flux increase per unit length (in the z direction) is

$$\phi_{10} = \phi_{21} = \phi_{32} = \text{---} = \frac{1}{2} \, s \, B_{10} \tag{6}$$

From Eq. (3)

$$T_{10} = T_{21} = T_{32} = \text{---} = T_o + \frac{J_{bo}}{c(T_o)} \, \phi_{10} \tag{7}$$

and therefore

$$J_{21} = J_{32} = J_{43} = \text{---} = J(T_{21}, B_{21}) \tag{8}$$

Finally

$$B_{20} = B_{31} = B_{42} = \text{---} = B_{21} + \mu_o \, s \, J_{21} \tag{9}$$

The succeeding values of flux increase to be substituted in Eq. (3) can be easily determined (see Eq. 10). This calculation procedure which can be continued in a similar way shows that for the case of a semi-infinite slab the distributions of B, T, and J inside the wave move along with the wave; that is, B, T, and J are functions of x only.

It would be possible to write a computer code based on Eq. (4) to (9). In the special case of a slab the distributions can be expressed in a closed form if we replace the general expression c(T,B) in Eq. (3) by Eq. (14). Then we can proceed as follows:

We consider the wave positions ξ_k, ξ_{k+1}. The flux increase $\phi_{k+1,\,\ell} - \phi_{k,\ell}$ is the difference between the areas bounded by the curve segments k + 1 and k. Therefore (see Fig. 1),

$$\phi_{k+1,\,\ell} - \phi_{k,\ell} = \frac{s}{2} \left(B_{k+1,\,\ell} + B_{k+1,\,\ell+1}\right) \tag{10}$$

Going to the limit $s \to dx$, Eqs. (3) (for the case of a semi-infinite slab, $2\pi R$ must be omitted) and (10) yield

$$J d\phi = J \, B \, dx = \frac{1}{\mu_o} \frac{\partial B}{\partial x} \, B \, dx = \frac{B}{\mu_o} \, dB = c(T) \, dT \tag{11}$$

Therefore for any distance x inside the wave the relation

$$\frac{B^2}{2\mu_o} = \int_{T_o}^{T} c(T) \, dT \tag{12}$$

is valid. This equation applied to the surface of the superconducting slab is the flux jump condition given by Wipf and Lubell.[1]

[1] S. L. Wipf and M. S. Lubell, Phys. Letters, 16, 103 (May 15, 1965).

In order to determine the functions B(x), T(x) and J(x), we make the following assumptions:

(a) In the range of interest the critical temperature T_c can be approximated by

$$T_c = T_{co} - bB \tag{13}$$

T_{co} is the critical temperature at B = 0

(b) The specific heat c for Nb-Zr can be approximated by

$$c = kT^4 \tag{14}$$

For Nb-25% Zr, k = 4.65 joule m^{-3} $(^oK)^{-5}$ (see Ref. 2).

(c) Experiments show that

$$J(T, B) = J_{bo} \frac{T_c - T}{T_c - T_o} f(B) \tag{15}$$

is a good approximation.

f(B) is a constant if the model of C. P. Bean and H. London is used. For Kim's model

$$J = J_{bo} \frac{T_o - T}{T_c - T_o} \cdot \frac{B_o}{B_o + B} \tag{16}$$

(d) The external field is raised fast enough to be almost adiabatic, but slow compared with the electromagnetic diffusion time.[3]

Considering Eq. (13), (14), (15) we obtain

$$dx = \frac{1}{\mu_o J_{bo}} \frac{T_{co} - T_o - bB}{T_{co} - bB - \left(\frac{5 B^2}{2 k \mu_o} + T_o\right)^{1/5}} \frac{dB}{f(B)} \tag{17}$$

We integrated this equation for various forms of f(B) and $T_o = 4.2^oK$ (Fig. 2). If the external field is very slowly raised, the isothermal wave front (Fig. 2a) results. In Fig. 3 isothermal (solid lines) and

---

[2] A. El Bindari and M. M. Litvak, J. Appl. Phys. 34, 2913 (1963).

[3] Y. B. Kim, C. F. Hempstead, and A. R. Strnad, Phys. Rev. Letters 13, 794 (1964).

adiabatic (dotted lines) flux distributions are compared for different positions ξ of the wave front.

Equation (12) holds strictly only if the wave front does not hit a boundary before the flux jump condition has been reached. For $T = T_c$, the current density J becomes zero and therefore ξ approaches ∞. Keeping this fact in mind the following condition for the temperature dependence of B_{FJ}, the external flux density when flux jump occurs is obtained from Eq. (17).

$$bB_{FJ} + \left(\frac{5\, B_{FJ}^2}{2\, k\, \mu_o} + T_o^5\right)^{1/5} = T_{co} \qquad (18)$$

This dependence is represented in Fig. 4.

Experiments show that the B_{FJ} values calculated by Eq. (18) are about 15% higher than the measured values. This deviation is mainly due to assumption (b) where the specific heat function is approximated by Eq. (14) which holds for B = 0. But it can be shown that for high κ materials and low fields, c(T, B) falls below c(T, 0) at higher temperatures[4]). Another possible explanation for the high calculated B_{FJ} values is the neglect of the normal eddy currents, but we estimate that these losses are small. Furthermore, when the external field H approaches B_{FJ}/μ_o, the velocity $\frac{d\xi}{dt}$ becomes so large that the assumption (d) is no longer valid. However, a very large increase of $\frac{d\xi}{dt}$ is caused by a very small increase of H, so that the value of B_{FT} is not appreciably influenced.

---

[4] L. Vieland and A. W. Wicklund (Unpublished).

III. FIELD DISTRIBUTIONS IN CYLINDERS

For superconducting cylinders the distributions of quantities B, T, and J are not functions of x alone and, therefore, do not move undistorted with the flux wave. We have developed a numerical integration method similar to that described previously for the semi-infinite slab. It is based on Eqs. (3) and (13) to (16). By means of a computer program, flux density distributions shown in Fig. 5 have been determined. The assumptions are the same as for Fig. 2c.

If the wave reaches the axis of a solid on the inner surface of a hollow cylinder, the computation procedure must be modified. Small arbitrary steps of B on the inner boundary are assumed which lead to ϕ, T, and J values in a similar way as described above. It is also possible to consider initially trapped fields. Figure 6a shows the flux distribution in a hollow cylinder with previously trapped flux. Figure 6b represents the case of initially trapped flux. The cross-hatched areas indicate the adiabatic flux changes. Additional computer results compared with experimental data will be published at another time.

After finishing this manuscript, we became aware of unpublished work by P. S. Swartz and C. P. Bean which discusses other aspects of this problem.

ORNL-DWG 65-8965

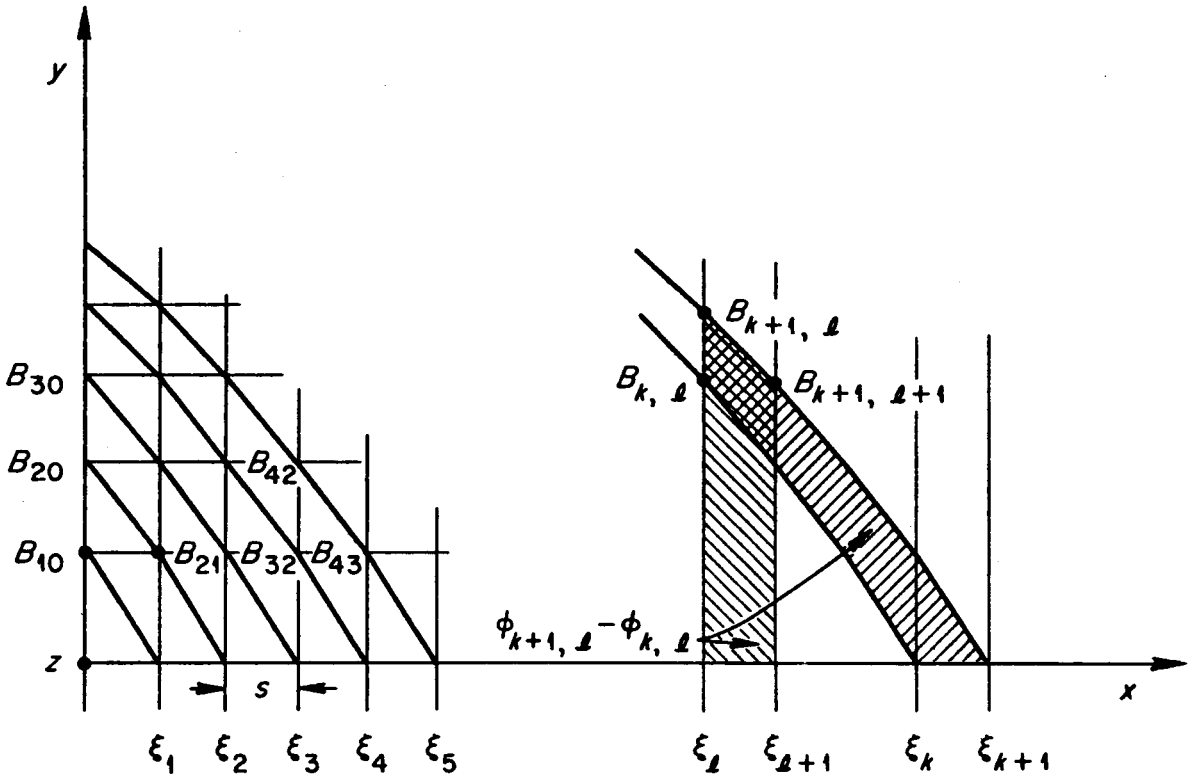

Fig. A-1. Step by Step Calculation of the B-Distribution in a Semi-Infinite Slab.

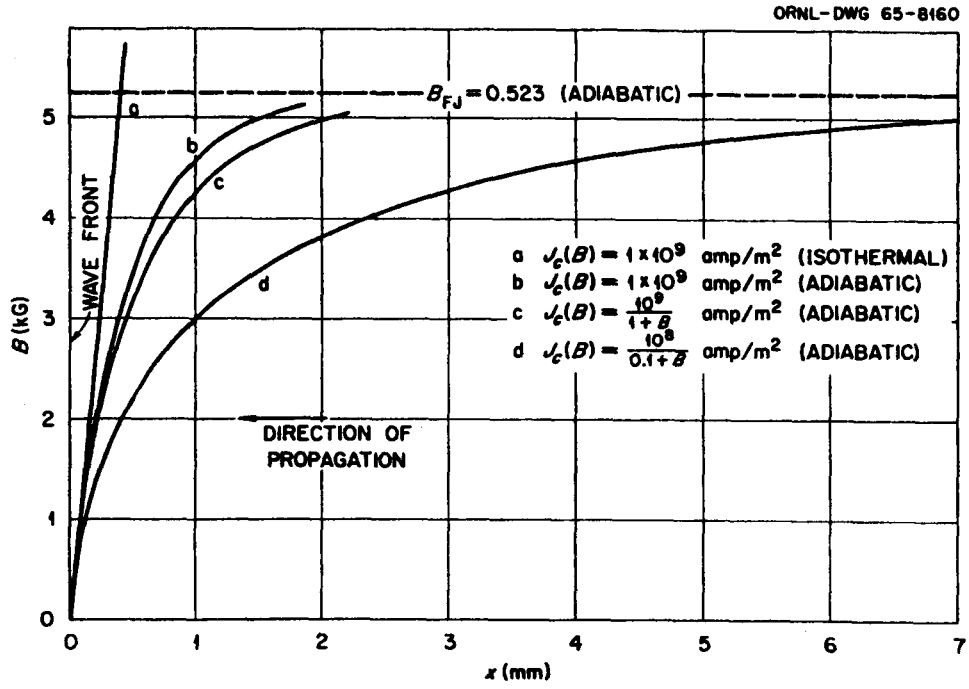

Fig. A-2. Magnetic Wave in a Slab of Nb-25% Zr, Flux Density B vs Distance x from the Wave Front.

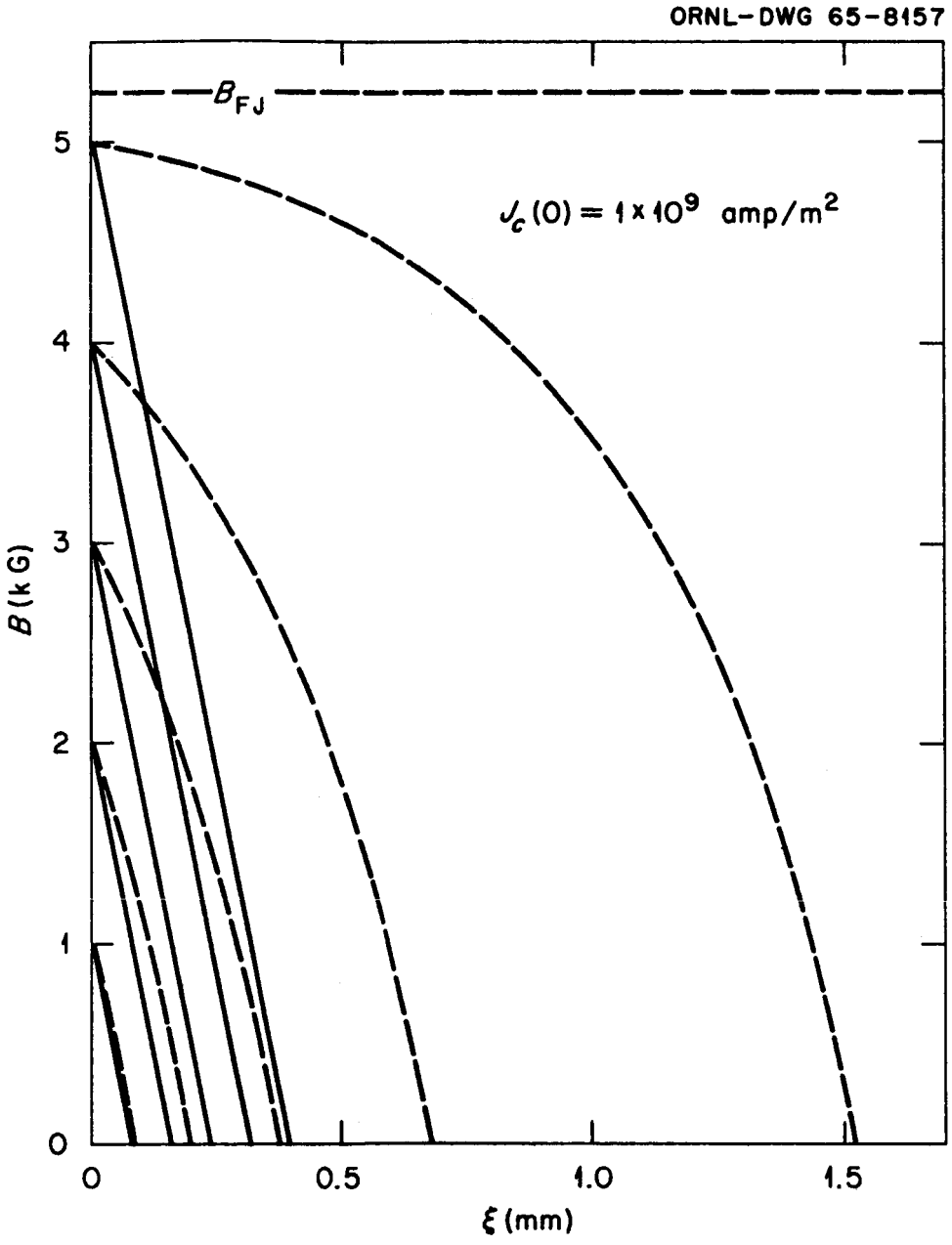

Fig. A-3. Flux Distribution for Isothermal and Adiabatic Field Changes in a Nb-25% Zr Slab.

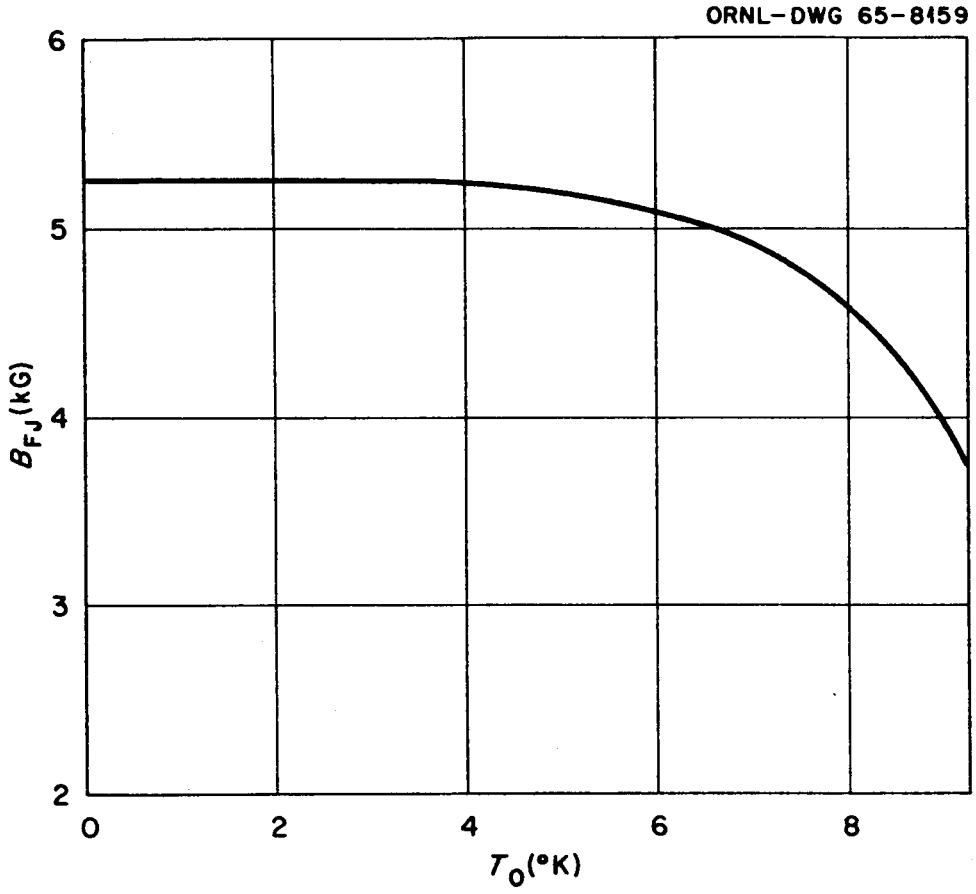

Fig. A-4. Dependence of B_{FJ} on the Bath Temperature T_o.

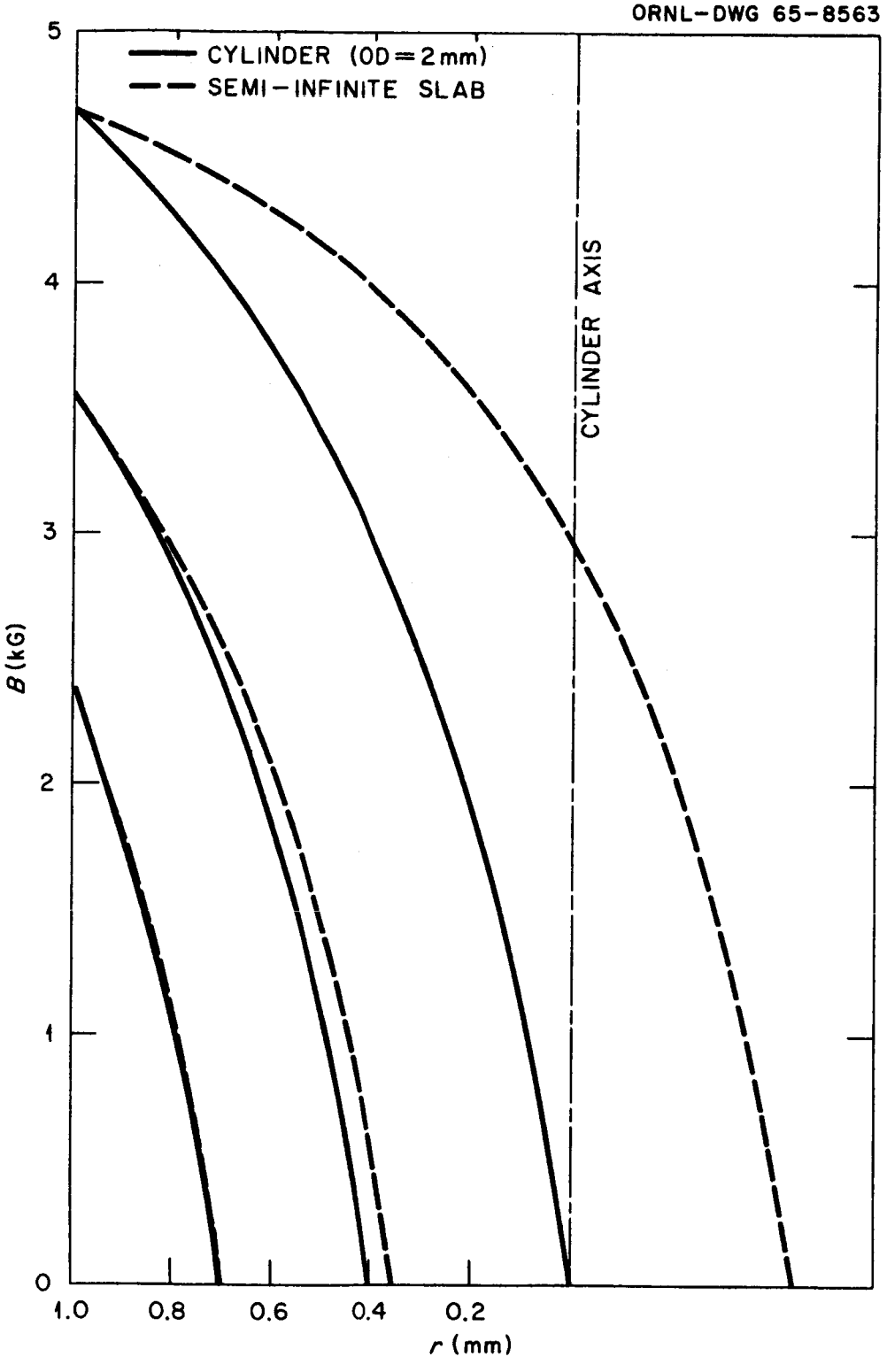

Fig. A-5. Flux Distribution for Adiabatic Field Change in Nb-25% Zr.

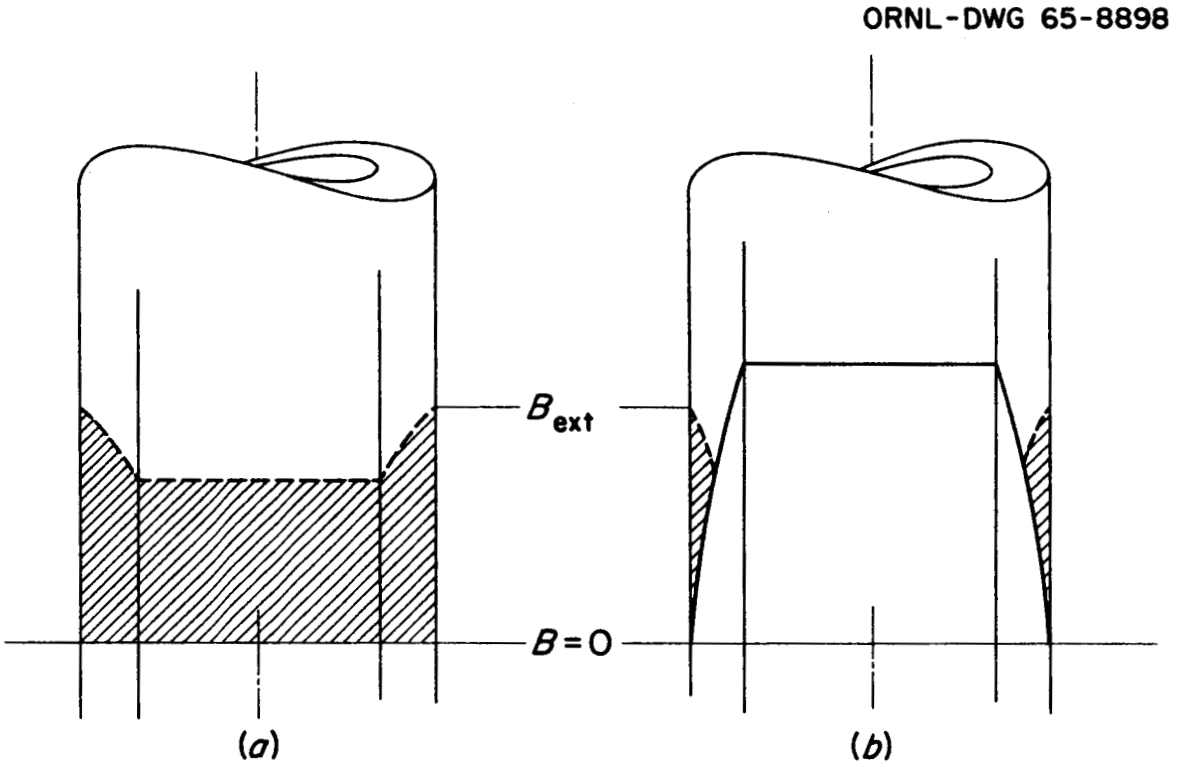

Fig. A-6. Flux Distribution in a Hollow Cylinder Without and With Initially Trapped Flux.

DISTRIBUTION LIST - REPORT JUNE 1 - AUGUST 31, 1965

Contract H-76798

	Addressee	Number of Copies
1.	George C. Marshall Space Flight Center Huntsville, Alabama 35812 Attn: Dr. J. C. Ashley Dr. E. W. Urban	40
2.	U. S. Atomic Energy Commission Oak Ridge, Tennessee Attn: Division of Technical Information	15
3.	U. S. Atomic Energy Commission Washington 25, D. C. 20545 Attn: Mr. William C. Gough	3
4.	Princeton University Princeton, New Jersey Attn: Dr. R. G. Mills	1
5.	Pennsylvania State University University Park, Pennsylvania Attn: Dr. F. G. Brickwedde	1
6.	Lawrence Radiation Laboratory Livermore, California Attn: Dr. C. Van Atta	1
7.	Los Alamos Scientific Laboratory Los Alamos, New Mexico Attn: Dr. J. L. Tuck Dr. H. L. Laqueur	2
8.	Massachusetts Institute of Technology National Magnet Laboratory Cambridge 39, Massachusetts Attn: Dr. H. H. Kolm Mr. D. B. Montgomery Dr. D. J. Rose Dr. J. Wulff	4
9.	Oak Ridge National Laboratory Oak Ridge, Tennessee Attn: Mr. A. J. Miller	1

Contract H-76798

Addressee	Number of Copies
10. Brookhaven National Laboratory Upton, New York Attn: Dr. J. E. Jensen Dr. A. G. Prodell	2
11. Iowa State University Ames, Iowa Attn: Dr. C. A. Swenson Dr. T. F. Stromberg	2
12. Argonne National Laboratory Argonne, Illinois Attn: Mr. C. E. Laverick	1
13. NASA-Lewis Research Center Cleveland, Ohio 44135 Attn: Mr. J. C. Laurence Mr. J. C. Fakan	2
14. Cryogenic Properties of Solids Cryogenic Engineering Laboratory National Bureau of Standards Boulder, Colorado 80301 Attn: Dr. Richard H. Kropschot	1
15. U. S. Naval Research Laboratory Washington, D. C. Attn: Dr. J. Babiskin	1
16. Oak Ridge National Laboratory Oak Ridge, Tennessee	
Attn: Central Research Library	2
Document Reference Section	2
Laboratory Records	2
ORNL-RC	1
W. F. Gauster	30
ORNL Patent Office	1
17. U. S. Atomic Energy Commission Oak Ridge, Tennessee Attn: Division of Research and Development	1